AIP | Review of Scientific Instruments

TetraMag: A compact magnetizing device based on eight rotating permanent magnets

M. Gilbert, H.-Ch. Mertins, M. Tesch, O. Berges, Herbert Feilbach, and C. M. Schneider

Citation: Review of Scientific Instruments **83**, 025109 (2012); doi: 10.1063/1.3684877
View online: http://dx.doi.org/10.1063/1.3684877
View Table of Contents: http://scitation.aip.org/content/aip/journal/rsi/83/2?ver=pdfcov
Published by the AIP Publishing

TetraMag: A compact magnetizing device based on eight rotating permanent magnets

M. Gilbert,[1,a)] H.-Ch. Mertins,[1] M. Tesch,[1] O. Berges,[1] Herbert Feilbach,[2] and C. M. Schneider[2,3]

[1]*University of Applied Sciences Münster, Stegerwaldstrasse 39, D-48565 Steinfurt, Germany*
[2]*Peter Grünberg Institut (PGI-6), Forschungszentrum Jülich GmbH, D-52425 Jülich, Germany*
[3]*Fakultät f. Physik and Center for Nanointegration Duisburg-Essen (CeNIDE), Universität Duisburg-Essen, D-47048 Duisburg, Germany*

(Received 6 October 2011; accepted 25 January 2012; published online 14 February 2012)

In this paper we describe a novel magnetizing device based on eight rotatable permanent magnets arranged in a quadrupolar configuration, which is termed the TetraMag. TetraMag creates stable and homogeneous magnetic fields at the sample position with a resolution of 0.02 mT tunable between –570 mT and +570 mT. The field direction is continuously rotatable between 0° and 360° within the sample plane, while the field strength is maintained. A simplified mathematical description of TetraMag is developed leading to magnetic field calculations which are in good agreement with the experimental results. This versatile device avoids electrical energy dissipation, cooling mechanisms, and hysteresis effects known from classical electromagnets. It is ultrahigh vacuum compatible and it offers a completely free optical path over 180° for magneto-optical experiments. It is suitable for scattering experiments with synchrotron radiation and neutrons and may be employed in a large class of magnetization experiments. © *2012 American Institute of Physics*. [http://dx.doi.org/10.1063/1.3684877]

I. INTRODUCTION

Magnetizing techniques, i.e., approaches which allow to vary and reverse a sample magnetization in a defined manner by means of external magnetic fields, are indispensable for the development of magnetic materials, sensors, or magnetic storage devices and for fundamental research in magnetism and spintronics.[1] Some of the most important experimental methods for the characterization of magnetic samples are based on the analysis of electrical and optical signals as a function of the sample magnetization. Among the optical methods the magneto-optical (MO) effects such as Faraday or Kerr effect play a key role. In these cases the intensity or the degree of polarization of the light beam after interaction with the magnetized sample is measured as a function of the magnetization,[2,3] which in turn is controlled by an external magnetic field $\vec{H}$. Commonly used magnetization devices involve solenoids, most often with soft iron yokes, which are arranged in dipole, quadrupole, or octupole geometry.[4–6] The ideal magnetization device offers the following features: (i) the magnetic field strength $|\vec{H}|$ is tunable, (ii) the field direction is rotatable in space, (iii) the field is stable with negligible ripple and homogeneous across the sample region of interest, and (iv) the sample is accessible over a wide angular range, e.g., for scattering experiments. Ideally, the magnetic field can be tuned with a negligible magnetic hysteresis. The thermal load should be negligible to facilitate the technical expenses. Last but not least ultra-high vacuum (UHV) compatibility is desirable due to the increasing amount of experiments exploiting synchrotron radiation.[2,7]

Classical electromagnets do not meet all of these requirements without compromising the available field strength. Due to their large pole pieces the sample is usually not accessible over the complete angular range from 0° to 180°, which restricts scattering experiments. In addition, the pole pieces are fabricated from ferromagnetic alloys with high saturation magnetization and permeability, which usually exhibit a hysteresis when scanning the magnetic field. In order to run an electromagnet under stable conditions an active cooling is necessary, which removes the Joule heat dissipated in the coils. Such a cooling circuit is complex and costly, in particular, for applications in the UHV. A rotation of the magnetic field $\vec{H}$ with respect to the sample – without rotating the entire magnet – is possible by a sophisticated octupole configuration, but this requires eight magnetic coils including eight power supplies and an elaborate electrical control system.[5] Hence, the costs of purchase and operation are high.

An interesting technical alternative to solenoids is provided by permanent magnets with a high energy product, i.e., preferentially of the NdFeB or CoSm type. In contrast to a solenoid, however, the magnetic field $\vec{H}$ produced by a permanent magnet at a given point in space can only be changed by moving the permanent magnet with respect to distance and/or orientation.[8] Because of the strong magnetic forces exerted between the permanent magnets, the mechanical layout of such a permanent magnet device is usually very bulky and costly.

In this paper, we describe a novel compact magnetizing device, based on a quadrupolar arrangement of eight transversely magnetized NdFeB permanent magnets of cylindrical shape which are symmetrically arranged in a square, and which can independently be rotated with respect to each other. This device which is called TetraMag due to its four pole piece geometry overcomes many of the technical problems of solenoid systems mentioned above. In Sec. II the principal configuration is depicted and a physical model is

a)Author to whom correspondence should be addressed. Electronic mail: gilbert@fh-muenster.de.

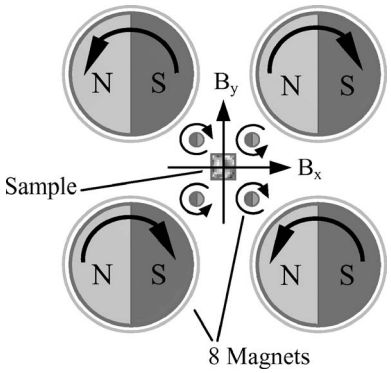

FIG. 1. Principal setup of the quadrupole magnetization device by diametrical magnetized cylindrical permanent magnets. The sample is placed in the center where the resulting magnetic field can be varied by rotating the permanent magnets about their longitudinal axes (front view).

presented which allows for the magnetic field calculation. Section III shows the mechanical setup of the TetraMag magnetizing device. Section IV documents the commissioning and compares experimental results with theoretical calculations. Finally, magneto-optical experiments are presented showing the potential of this novel approach.

II. CONCEPT AND THEORETICAL CONSIDERATIONS

In this paper the general concept of the novel magnetizing device based on the rotation of permanent magnets is outlined.

The core part of TetraMag comprises a set of 4 strong and a set of 4 weaker FeNdB permanent magnet blocks. Each magnet is a bar-shaped cylinder with a magnetization direction imprinted perpendicular to its longitudinal axis (Fig. 1). The four strong magnets are placed at the corners of a square. The weaker magnets are placed as well at the corners of a smaller square inscribed within the larger one. Both squares are centered with respect to the sample. At the sample the magnetic field contributions of all magnets are superimposed and add up to the resulting magnetic field $\vec{H}_{samp}$. The major field contribution arises from the strong magnets. The smaller magnets serve as field correctors to increase the field homogeneity at the sample position. In order to vary the magnetic field $\vec{H}_{samp}$ in magnitude and orientation each magnet can be rotated about its longitudinal axis (Fig. 1). Two different working modes are feasible: (a) the magnetic field direction is maintained and the field strength is tuned from maximum positive field across zero to maximum negative field and back and (b) which keeps the magnetic field strength constant, but rotates the field direction about the center. For each mode a specific coupling of all individual eight magnets is required, which is described in detail below.

In Sec. II A the theoretical description of the generation of the tunable magnetic field is evolved in several steps. First, the permanent magnet block is treated as a pointlike magnetic dipole and the field generated by four magnetic dipoles is calculated. This simple model facilitates the optimum geometrical arrangement of the bulky permanent magnets to be found. In Sec. II B we expand the description and focus on the rotation of the magnetic field in space. In Sec. II C the resultant field homogeneity is investigated and the improvement by adding further magnets is described. In Sec. II D the simple magnetic dipole model is substituted by a finite elements method (FEM) to calculate the resultant magnetic field of all bulky permanent magnets. The result shows that the simple dipole model is already a good approach for the field components at the sample position.

A. Model and field calculation

In this section we develop a simplified model for a description of the magnetic field distribution of the TetraMag device. The bulky magnetic cylinder is represented by a simple pointlike magnetic dipole with moment $\vec{m}$ (Fig. 2, left side). The field of a homogeneously magnetized cylinder is not identical to the field of a dipole. The moment $\vec{m}$ is oriented within the x-y-plane and we consider only points within this plane and this dipole model may appear to be too simplified at first glance. However, it already captures the salient features of the setup.

The resulting magnetic induction $\vec{B} = (B_x, B_y)$ at distance R with $R^2 = (x_1 - x_0)^2 + (y_1 - y_0)^2$ is expressed by Eqs. (1) and (2):

$$B_x = \frac{c}{R^3} 2\cos(\alpha - \beta)\cos\beta + \frac{c}{R^3}\sin(\alpha - \beta)\sin\beta, \tag{1}$$

$$B_y = \frac{c}{R^3} 2\cos(\alpha - \beta)\sin\beta - \frac{c}{R^3}\sin(\alpha - \beta)\cos\beta \tag{2}$$

with $c = m/4\pi$. The rotation of the permanent magnet corresponds to the rotation of this dipole by an angle α with respect to the x-axis. The rotation is measured counter clockwise positive. The coordinate system is spanned by the horizontal x-axis, the vertical y-axis lying in the sample surface plane, and the z-axis perpendicular to the sample surface.

In the next step we have to figure out how to arrange four magnetic moments to obtain an optimum resultant field B at the sample according to Eqs. (1) and (2). Positioning of four identical magnetic moments at the corners of a square emerges as the best solution from symmetry arguments (Fig. 2 right side). This arrangement leads to angles $\beta_1 = \pi/4$, $\beta_2 = 3\pi/4$, $\beta_3 = 5\pi/4$, and $\beta_4 = 7\pi/4$ with respect to the sample in the center at $(x = 0, y = 0)$. The resulting field vector at the samples position is deduced from Eqs. (1) and (2) to

$$\vec{B} = \sum_{i=1}^{4} \vec{B}_i = \begin{pmatrix} B_x \\ B_y \end{pmatrix} = \frac{c}{2R^3} \begin{pmatrix} 3\sin\alpha_1 + \cos\alpha_1 - 3\sin\alpha_2 + \cos\alpha_2 + 3\sin\alpha_3 + \cos\alpha_3 - 3\sin\alpha_4 + \cos\alpha_4 \\ 3\cos\alpha_1 + \sin\alpha_1 - 3\cos\alpha_2 + \sin\alpha_2 + 3\cos\alpha_3 + \sin\alpha_3 - 3\cos\alpha_4 + \sin\alpha_4 \end{pmatrix}. \tag{3}$$

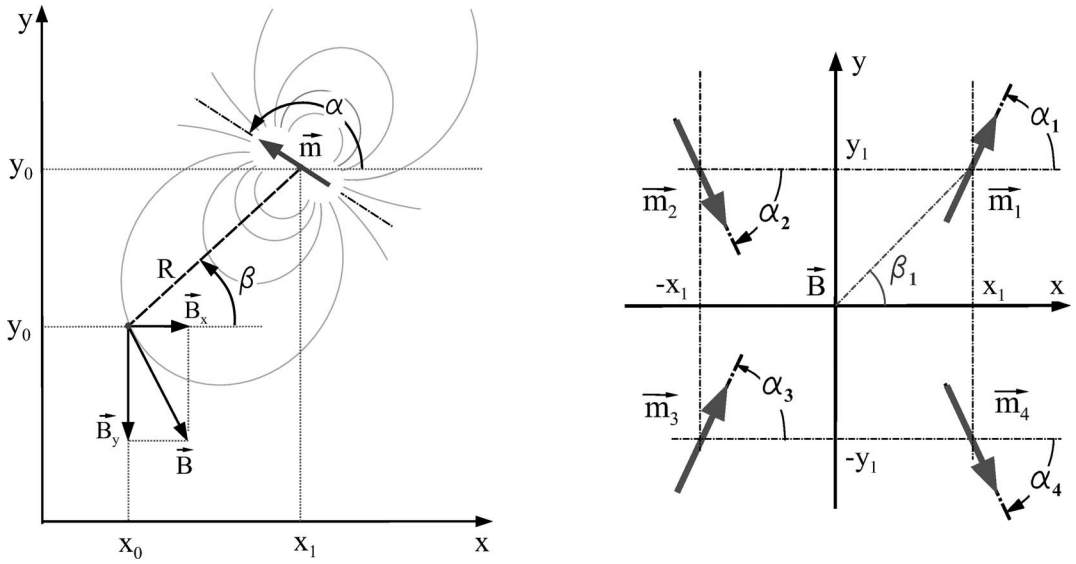

FIG. 2. Left: Relevant parameters for the field produced by one single magnet with magnetic moment $\vec{m}$. Right: Angles α_j of four rotatable permanent magnets (see Fig. 1), described by their magnetic moments $\vec{m}_j$. The sample rests in the coordinate center.

The field vector is located in the x-y-plane without any z-component. Now we deduce the requirements for a purely horizontal magnetic field B_x without any vertical component which means that the y-component of Eq. (3) has to vanish, i.e.,

$$(3\cos\alpha_1 + \sin\alpha_1 - 3\cos\alpha_2 + \sin\alpha_2 + 3\cos\alpha_3 + \sin\alpha_3 - 3\cos\alpha_4 + \sin\alpha_4) = 0. \quad (4)$$

As a consequence the four individual angles $\alpha_1, \alpha_2, \alpha_3$, and α_4 have to obey specific conditions which have to be determined. One possible solution is given by

$$\alpha_1 = \alpha_3, \quad \alpha_2 = \alpha_4, \quad (5a)$$

$$\alpha_1 = -\alpha_2, \alpha_3 = -\alpha_4. \quad (5b)$$

The first conditions $\alpha_1 = \alpha_3$ and $\alpha_2 = \alpha_4$ follow from symmetry consideration (see Fig. 2, right side) which leads to identical field contributions $B_{y1} = B_{y3}$ and $B_{y2} = B_{y4}$ at the samples position ($x = 0$, $y = 0$). The second condition (Eq. (5b)) describes the coupling of all four magnets. Both conditions ((5a) and (5b)) have to be maintained to vary the magnetic field strength with permanent field direction parallel to the x-axis. This means that a purely horizontal magnetic field at the sample can be obtained if the corresponding magnets rotate in the opposite direction and the rotation starts with $\alpha_1 = \alpha_2 = \alpha_3 = \alpha_4 = 0$. The resultant field component in x-direction is given by

$$B_x = \sum_{i=1}^{4} B_{xi} = 2\frac{c}{R^3}(3\sin\alpha_1 + \cos\alpha_1) = 2\sqrt{10}\frac{c}{R^3}\cos(\alpha_1 - \varepsilon) \quad (6)$$

with the abbreviation $\varepsilon = \arctan(3) = 71,565°$. Due to the coupling of all angles the resultant expression needs one angular variable (α_1) only. These calculations clearly show that, while the magnetic field direction is fixed a variation of the magnetic field strength from positive maximum value across zero to negative maximum value is possible by simply tuning the angles of all four magnets synchronously as depicted in Fig. 2, right side.

B. Field rotation

A second topic is the rotation of the magnetic field vector with the aim to keep its absolute value constant. For this feature two alternative technical options have been evaluated. The first option can be managed by a well-defined set of pinions, which couple all magnets to one single motor. This mechanical solution is described in Sec. III A.

The second option provides more flexibility through an individual control of each magnet. It requires eight motors to adjust the individual angle of each magnetic rod and it is described in the following. To realize a practicable device a procedure has to be developed that allows to select first a magnetic field strength $|\vec{B}|$ and second to rotate the magnetic field vector in the x-y-plane about the angle γ while the absolute value $|\vec{B}|$ is unchanged. The angle γ is to be measured counter clockwise with respect to the x-axis (not shown in Fig. 2). Therefore, the coupling condition for the rotating magnets, i.e., their individual angles $\alpha_1, \alpha_2, \alpha_3$, and α_4, has to be determined. One theoretical approach with limited degrees of freedom is discussed in Ref. 9. Here we choose a different way. It allows to set the x- and y-components of the magnetic field vector independently. According to Fig. 2, right side, the magnetic moments $\vec{m}_1$ and $\vec{m}_2$ are coupled to create one component of the resulting magnetic field vector, e.g., the vertical component B_y and the remaining two magnetic moments $\vec{m}_3$ and $\vec{m}_4$ are coupled to produce the horizontal component B_x. This solution enables to create variable magnetic fields in the x-y-plane. It has the advantage over different matchings, e.g., the diagonal pairing of $\vec{m}_1$ with $\vec{m}_3$ and $\vec{m}_2$ with $\vec{m}_4$ to yield the maximum available field strength $|\vec{B}|$. The magnetic field which is created by the paired moments $\vec{m}_1$ and $\vec{m}_2$ is given

by

$$\vec{B}_1 + \vec{B}_2 = \frac{c}{2R^3}\begin{pmatrix} 3\sin\alpha_1 + \cos\alpha_1 - 3\sin\alpha_2 + \cos\alpha_2 \\ 3\cos\alpha_1 + \sin\alpha_1 - 3\cos\alpha_2 + \sin\alpha_2 \end{pmatrix}. \tag{7}$$

To obtain a purely vertical magnetic field the individual angles have to be coupled by $\alpha_2 = \pi - \alpha_1$. The contributions of the magnetic moments $\vec{m}_3$ and $\vec{m}_4$ result in

$$\vec{B}_3 + \vec{B}_4 = \frac{c}{2R^3}\begin{pmatrix} 3\sin\alpha_3 + \cos\alpha_3 - 3\sin\alpha_4 + \cos\alpha_4 \\ 3\cos\alpha_3 + \sin\alpha_3 - 3\cos\alpha_4 + \sin\alpha_4 \end{pmatrix}. \tag{8}$$

A purely horizontal field is obtained for the coupling condition $\alpha_4 = -\alpha_3$. Both coupling conditions and the relevant equations (7) and (8) lead to

$$\vec{B} = \sum_{i=1}^{4}\vec{B}_i = \frac{c}{R^3}\begin{pmatrix} 3\sin\alpha_3 + \cos\alpha_3 \\ 3\cos\alpha_1 + \sin\alpha_1 \end{pmatrix}. \tag{9}$$

Next a calculation rule has to be deduced which gives the values of α_1 and α_3 for the desired angle γ of the resulting magnetic field vector. In an intermediate step the boundary condition $|\vec{B}|^2 = (\Sigma_i B_{xi})^2 + (\Sigma_i B_{yi})^2 = \text{const.}$ has to be considered which leads with Eq. (9) to

$$\alpha_1 = \arcsin\sqrt{\frac{|\vec{B}|^2 R^6}{10c^2} - \cos^2(\alpha_3 - \varepsilon)} - \varepsilon. \tag{10}$$

This expression is a function of the desired magnetic field strength with the abbreviation $\varepsilon = \arctan(3)$ and the above-mentioned conditions $\alpha_1 = \pi - \alpha_2$ and $\alpha_3 = -\alpha_4$.

Before deducing the final formula including both, the angle γ and the magnetic field strength as relevant parameters, the maximum adjustable magnetic field strength has to be discussed.

Equation (10) shows that the achievable maximum magnetic field strength is limited. For the special situation $\gamma = \pi/4$ with identical x- and y- components of the magnetic field the maximum value is limited by $|\vec{B}| \le \sqrt{2}\sqrt{10}c/R^3$. For the general situation $0 \le \gamma \le 2\pi$ the maximum achievable field is reduced to $|\vec{B}| \le |\vec{B}|_{\max} = \sqrt{10}c/R^3$. This results from the fact that apart from $\gamma = \pi/4$ the x- or y-component has to increase up to this maximum value. As a consequence the working mode for field rotation about γ reduces the maximum achievable field strength by a factor of two compared to the mode of tuning the magnetic field with purely horizontal direction (Sec. II A, Eq. (6)).

The concluding step leads to a calculation rule for the values α_1, α_2, α_3, and α_4 as a function of the desired angle γ and the magnetic field vector which is given by

$$\alpha_3 = \arccos\left(\frac{|\vec{B}|R^3}{\sqrt{10}c}\cos\gamma\right) + \varepsilon, \tag{11a}$$

$$\alpha_1 = \arcsin\left(\frac{|\vec{B}|R^3}{\sqrt{10}c}\sin\gamma\right) - \varepsilon, \tag{11b}$$

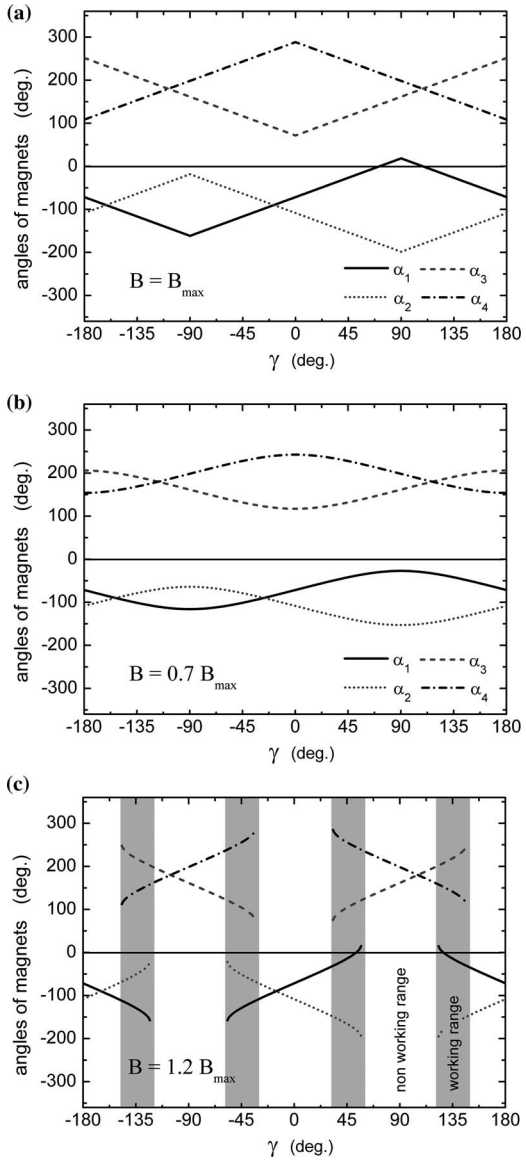

FIG. 3. Calculation rule for the angular values α_1, α_2, α_3, and α_4 of the field producing magnets (Fig. 2) as a function of the desired angle γ and the magnetic field. Only for limited field strengths $0 \le |B| \le |B|_{\max}$ the full tuning range $0 \le \gamma \le 2\pi$ can be covered ((a) and (b)). For larger fields $|B| > |B|_{\max}$ the accessible range of γ is restricted ((c)).

$$\alpha_4 = -\alpha_3, \tag{11c}$$

$$\alpha_2 = \pi - \alpha_1. \tag{11d}$$

These four angles are plotted as a function of γ for different magnetic field strengths in Figs. 3(a)–3(c). The general situation $0 \le |B| \le |B|_{\max}$ is shown in Fig. 3(b). The angle γ can be tuned from 0 to 2π without any limitation. The plotted functions give the instruction to drive the four magnets (Fig. 2) mechanically. Figure 3(a) shows these functions for the maximum achievable field strength $|B| = |B|_{\max}$. Beyond this limit a continuous tuning of γ is impossible and the operation is reduced to small angular ranges. With increasing field strength the working range decreases to $\gamma = 45°$, 135°, 225°, 315° where both magnetic field components B_x and B_y are identical.

C. Magnetic field profile

In this section the magnetic field strength as a function of the position x is deduced with the purpose to achieve the field homogeneity along the x-axis (i.e., $y = 0$). Note that the notation will be changed in the following discussion by $x_0 = x$. Using the parameters defined in Fig. 1, we deduced Eq. (1) for one single dipole. With dipole position (x_1, y_1) and the relations $\sin\beta = y_1/R$, $\cos\beta = (x_1 - x)/R$, and $R = \sqrt{y_1^2 + (x_1 - x)^2}$ the relevant field strength at the position (x, y) is found to be

$$B_x(x) = \frac{c}{R^5}\left(3y_1(x_1 - x)\sin\alpha_1 - y_1^2\cos\alpha_1 + 2(x_1 - x)^2\cos\alpha_1\right). \quad (12)$$

For the TetraMag device (Fig. 1) four dipoles are used with the positions $(x_1 = a, y_1 = a)$, $(x_2 = -a, y_2 = a)$, $(x_1 = -a, y_3 = -a)$, and $(x_4 = a, y_4 = -a)$. The resulting field strength at the position $(x, y = 0)$ follows from Eq. (12) for each of these four dipoles and the formerly deduced Eqs. (5a) and (5b), and it is given by

$$\sum_{i=1}^{4} B_{xi}(x) = 2c\left(\begin{array}{l}\frac{1}{\sqrt{a^2+(a-x)^2}^5}(3a(a-x)\sin\alpha_1 - a^2\cos\alpha_1 + 2(a-x)^2\cos\alpha_1)\ldots \\ \cdots + \frac{1}{\sqrt{a^2+(a+x)^2}^5}(3a(a+x)\sin\alpha_1 - a^2\cos\alpha_1 + 2(a+x)^2\cos\alpha_1)\end{array}\right). \quad (13)$$

The profile $B_x(x)$ is plotted in Fig. 4 right side (dashed line). The purpose of the above considerations and coupling conditions of the four dipoles is the creation of a horizontal magnetic field $\vec{B} = (B_x, B_y = 0)$. It can be shown that the component B_y vanishes not only at the center point $(x = 0, y = 0)$ but also along the complete y-axis, i.e., at $(x = 0, y \neq 0)$ and along the complete x-axis, i.e., $(x \neq 0, y = 0)$. This will not be deduced in detail but it follows from symmetry considerations (Fig. 1) and due to the fact that the dipoles rotate in the opposite directions which cancels out the y-components.

D. Improvement of the field homogeneity

Figure 4 right side (dashed line) shows a fast decrease of the field strength near the center position which is not suited to magnetize larger samples homogenously. To obtain a wide homogenous field which covers the complete sample, four further magnets are added. This improvement will be discussed in this section.

The gradient $\partial B/\partial x$ has to be reduced while the absolute field strength $\sum B_x$ has to be unaffected. Figure 4 right side shows the additional four magnets m_5 to m_8, which are weaker than the four strong magnets but as well magnetized diametrically. These are placed on the interior square with center at $(x = 0, y = 0)$ as shown in Fig. 4, left side. These four weaker magnets create a second field contribution, pointing in x-direction if the coupling condition $\alpha_6 = -\alpha_5$, $\alpha_8 = -\alpha_7$, $\alpha_5 = \alpha_7$, and $\alpha_8 = \alpha_6$ is provided according to the coupling conditions of the stronger magnets. The angles α_{5-8} are defined analogously in Fig. 2, right side. If the orientation between stronger and weaker magnets is given by $\alpha_5 = 2\varepsilon - \alpha_1$ with $\varepsilon = \arctan(3)$, all eight magnetic contributions B_x point into the same direction. Additionally, the curvature of the magnetic field contribution of the weaker magnets is opposite to that of the stronger magnets. The magnetic field homogeneity exhibits best performance if the inner, weaker magnets and the outer, stronger magnets obey the relation

$$\left|\frac{d^2}{dx^2}B_{x\text{inner}}\right| = \left|\frac{d^2}{dx^2}B_{x\text{outer}}\right|. \quad (14)$$

From Eqs. (13) and (14) the relation between the relative magnetic dipole strength $m_{\text{inner}}/m_{\text{outer}}$ and the relative position $a_{\text{inner}}/a_{\text{outer}}$ of the relevant magnets is deduced to

$$\frac{m_{\text{inner}}}{m_{\text{outer}}} = \left(\frac{a_{\text{inner}}}{a_{\text{outer}}}\right)^5. \quad (15)$$

The resulting field distribution is shown in Fig. 4, right side for the special case: $B_x = 0$ and $a_{\text{inner}}/a_{\text{outer}} = 0.5$. The contribution of the four weaker magnets is shown by the grey line. This additional contribution leads to an enlarged homogeneity of the total magnetic field across the center (full line) compared to the situation with one magnetic quadrupole (dashed line). The positions of the inner magnets are given by $(\pm a/2)$, $(\pm a/2)$.

A further outcome of the above consideration is the fact that the homogeneity in y-direction is improved as well. From the condition $divB = 0$ for magnetic fields the requested condition $\partial B/\partial x = 0$ leads also to $\partial B/\partial y = 0$ which describes the homogeneity in y-direction.

E. Numeric simulation

The model discussed above was concerned with eight pointlike magnetic dipoles. In practice, instead of these simplified objects long diametral magnetized rods are used. Their diameter and length determine the resultant magnetic field at the sample position. To account for the magnetic volume we used the FEM calculation software COMSOL© (Ref. 10) (finite element method). Each rod is treated as a homogenous magnet with magnetization $\vec{M}$. The magnetization is connected to the magnetic source density via $\sigma_{mag} = div\vec{M}$ (see Ref. 11). In turn the source density is connected to the scalar magnetic potential at a point x at a distance $x - x_{0j}$

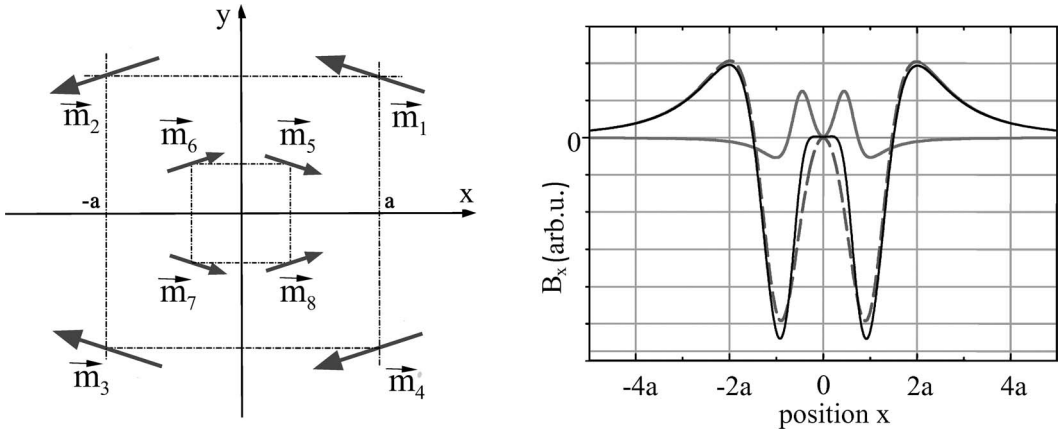

FIG. 4. Left: Arrangement of four strong magnets located on an outside square with side length $2a$. Four weak magnets on an inside square with side length $2(a/2)$ serve for increased homogeneity. Right: Magnetic field on the x-axis as a function of relative position x. Dashed line: Contribution of 4 strong magnets m_1 to m_4; grey line contribution of 4 weak magnets m_5 to m_8; full line total field.

measured with respect to a point x_{0j} on the surface of the magnetic rod with surface element of size A, which is given by $\phi(x) = -(1/4\pi)\sum_j (\sigma_{mag}(x_{0j})/|x - x_{0j}|)A_j$. From this potential the resultant magnetic field is deduced via $\vec{B} = -\mu_0 grad\phi$ (see Ref. 11). In this way the full vector of the magnetic field for each point (x, y, z) of the three-dimensional space around the sample can be calculated.

A plot of the magnetic field profile computed in the sample plane is shown in Fig. 5. We can clearly see the improvement of field homogeneity in the central region due to the additional four small magnets. Essentially, these finite element calculations confirm the conclusions drawn from the point dipole model.

III. THE TETRAMAG MAGNETIZING DEVICE

Two different types of quadrupole magnetizing devices have been realized. The first one uses one single motor to drive the magnets, which are coupled via a fixed set of pinions. The second type uses eight motors for an individual control of each magnet.

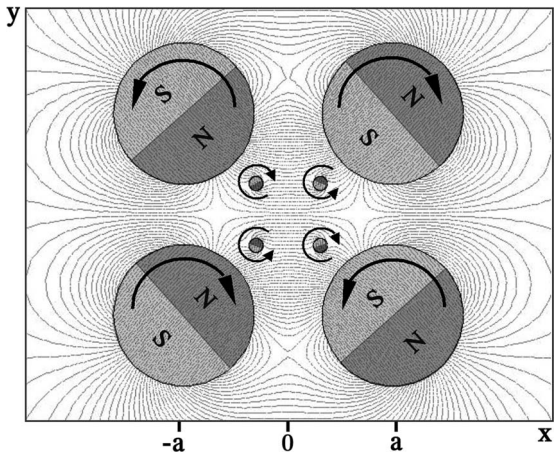

FIG. 5. FEM calculation of the magnetic field profile in the sample plane x-y with $z = 0$.

A. Type A: Coupled magnets

A perspective view of the mechanical construction is shown in Fig. 6(a) and a photograph of the setup is found in Fig. 6(b). The four strong magnetic rods with diameter 60 mm and length 130 mm are centered at the corners of a square with side length $2a = 95$ mm. Each rod is made up of three cylindrical NdFeB magnets with a remanence field of $B_R = 1.35$ T. The four weaker magnetic rods with 7 mm diameter and length 120 mm are arranged in a square with side length $2a = 28$ mm. Their remanence field is again $B_R = 1.35$ T. The sample is placed in the center of the squares with respect to the front view and also with respect to the side view. The latter positioning guarantees a homogenous magnetic field also with respect to the z-direction.

Note that this geometrical arrangement most naturally leads to a full optical access to the sample within the horizontal and vertical direction. The magnets are held in place in a solid frame. The backside of the frame carries the gear mechanisms to move the magnets. An appropriate coupling of these gears according to Eqs. (5a) and (5b) allows for a drive mechanism, which needs one motor only. The complete device is placed on a goniometer for optical reflection experiments, e.g., magneto-optical Kerr effect measurements. This enables one to tune the incidence angle θ of the impinging light beam in the horizontal plane with respect to the sample surface (Fig. 6(a)). The reflected beam is collected on a detector that rotates on a second goniometer by about 2θ. Due to the assembly by long magnetic rods, any scattering angle between grazing incidence ($2\theta = 0°$) and normal incidence ($2\theta = 180°$) in the horizontal plane can be set. This is usually not possible by conventional electromagnets. For applications in an UHV the complete device is installed in an appropriate UHV chamber.

The rotation of the magnetic field vector in the sample surface plane can be managed by the above described gear system. For this purpose two conditions have to be fulfilled: the construction of the magnetic assembly must be separated from the sample support and the magnetic assembly must be mounted in a large vertical pivot bearing (Figs. 6(a) and 6(b)). Thereby, the entire system of eight magnets can be rotated

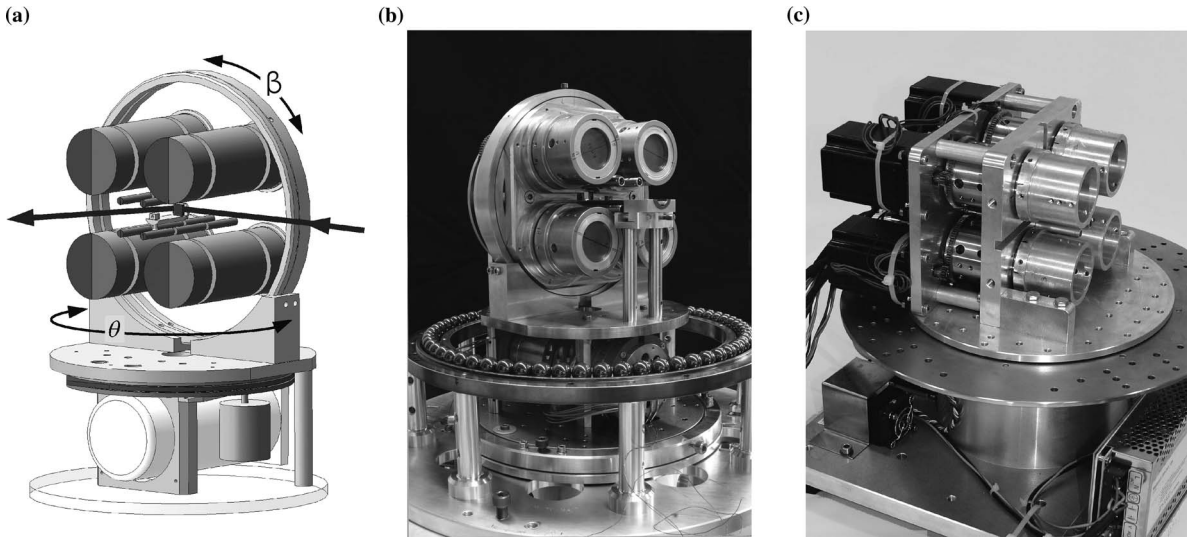

FIG. 6. (a) Design drawing of the quadrupole magnetization device showing 4 large and 4 small magnetic rods with the sample placed in the center. The gear pinions at the back side are not shown. For magneto-optical experiments any angle of incidence for the light beam can be set by rotating the complete device about theta. (b) Photograph with base frame and opened goniometer. (c) Photograph of device type B (details see text).

about the angle β (Figs. 6(a) and 6(b)), which corresponds to a rotation axis perpendicular to the sample surface while the sample is held fixed in space. Because the relative orientation of all eight magnets with respect to each other is fixed, the absolute value of the magnetic field does not change and simply the magnetic field vector is rotated about β. This rotation about β is based on a sophisticated mechanics. A screw has to be removed which locks the large vertical pivot bearing (Figs. 6(a) and 6(b)). As a result the motor can move the complete system while the individual magnets are fixed with respect to each other due to the strong intermediate magnetic forces. This modus allows for a magnetic field rotation in the sample plane within the range $0^\circ \leq \beta \leq 90^\circ$. The locking screw can be fixed for $\beta = 0^\circ$ and for $\beta = 90^\circ$. In these positions, which correspond to longitudinal (horizontal) and transversal (vertical) field, respectively, the absolute value of the magnetic field can be tuned by driving the motor as described above.

The mechanical forces due to the magnetic attraction or repulsion between the individual magnets are below 300 N. The maximum torque needed is 100 Nm. These values determine the details of the mechanical construction, the layout of the bearings, and the strength of the motor. Both types ceramic ball bearings and friction type bearings have been used. Further specifications have to be achieved concerning UHV compatibility: the bearings are lubricated with special UHV-compatible grease.[12] The motor is an UHV stepper motor, type Phytron VSS80. The gear pinions are coated with WS_2. The construction material is mainly stainless steel (type 1.4571) or with low magnetic susceptibility, beryllium copper which avoids a spatial deformation of the magnetic field. All trapped volumes, e.g., blind holes, large flat bolted surfaces, etc. are provided with suitable pumping holes or grooves. The motor is connected via copper braids with a cooling system outside the vacuum chamber. As a result the outgassing rate during motor operation is reduced and the sample stays at room temperature, which is controlled additionally by a conventional NiCrNi thermoelement.

The resulting magnetic field vector is monitored by two UHV-compatible Hall sensors,[13] one for the x-direction (horizontal) and a second one for the y-direction (vertical). Both sensors are placed 3 mm behind the sample and have been calibrated with respect to the sample surface. For this purpose, a commercial Hall sensor, type Koshava-alpha was used. In combination with a computer control these sensors allow for a precise tuning of the magnetic field with an accuracy of $\Delta B \leq 0.02$ mT.

B. Type B: Individual magnetic drive

The mechanical setup and the positions of all eight magnets are identical to type A, described in Sec. III A. However, the magnets are not coupled by a set of pinions, but rather eight stepper motors are used to drive each magnet individually according to the procedure described in Sec. II. Figure 6(c) shows this magnetization device placed on a two axes goniometer.

IV. EXPERIMENTAL RESULTS

In Sec. IV A experimental results and specifications of the TetraMag magnetizing device are presented, while its potential for scientific investigations is demonstrated by means of magneto-optical spectroscopy on magnetic layers in Sec. IV B.

A. Magnetic field of type A

In the following the type A device is characterized where all eight magnets are coupled by an appropriate set of pinions to fit the conditions described in Sec. II. This allows one to drive the rotation angles α_j by one single motor. The magnetic field strength B_x (horizontal orientation) and B_y (vertical orientation) at the sample position as a function of the relative rotation angle α_j of the magnetic rods is shown

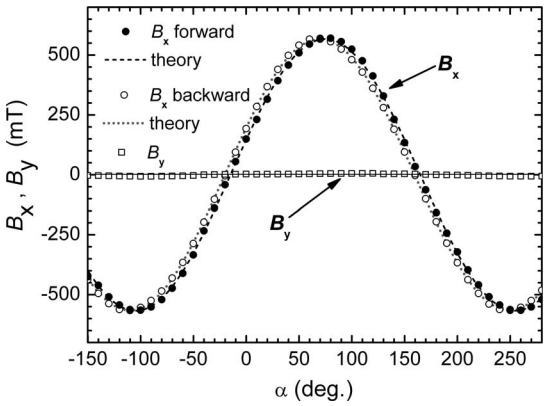

FIG. 7. Magnetic field strength B_x and B_y as function of the relative rotation angle of the magnetic rods (symbols: experimental results, line: calculation).

in Fig. 7 (symbols). A continuous variation of B_x is achieved with values between –570 mT and +570 mT with horizontal alignment of the field vector. As expected the angular dependence follows the theoretical predictions (Sec. II) as obtained by FEM simulations (lines). Experimental and calculated data agree closely in both, the absolute field strength and the angular position. This shows a good mechanical alignment of all magnets and an almost transmission-slip free bearing.

A reversal of the scan direction in this range leads to a small shift on the angular axis (circles in Fig. 7). This arises because of backlash of the gear system. However, this does not affect the practical application, because the actual magnetic field is determined by the above-mentioned Hall sensors within $\Delta B < 0.02$ mT. Therefore, this effect can be compensated by online control of the real magnetic field. To tune the full magnetic field range the practical operating range of the quadrupole magnetization device lies between 70° and 250° or between 70° and –100° rotation angle of the magnets (Fig. 7).

The homogeneity of the magnetic field in x-direction is depicted in Fig. 8. Each set of experimental data (symbols) constitutes a curved line. These are obtained for a fixed rotation angle α of the magnetic rods. The data are obtained by moving a Hall sensor horizontally. Best performance is obtained for intermediate field strengths, e.g., for 300 mT. A

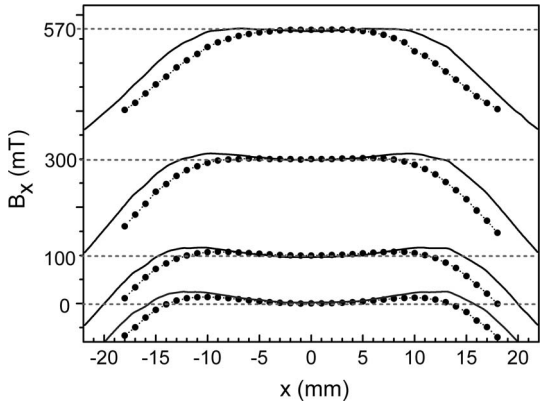

FIG. 8. Homogeneity of the magnetic field as a function of distance x from the center, shown for different field strengths B_x; symbols: experimental data, lines: calculations.

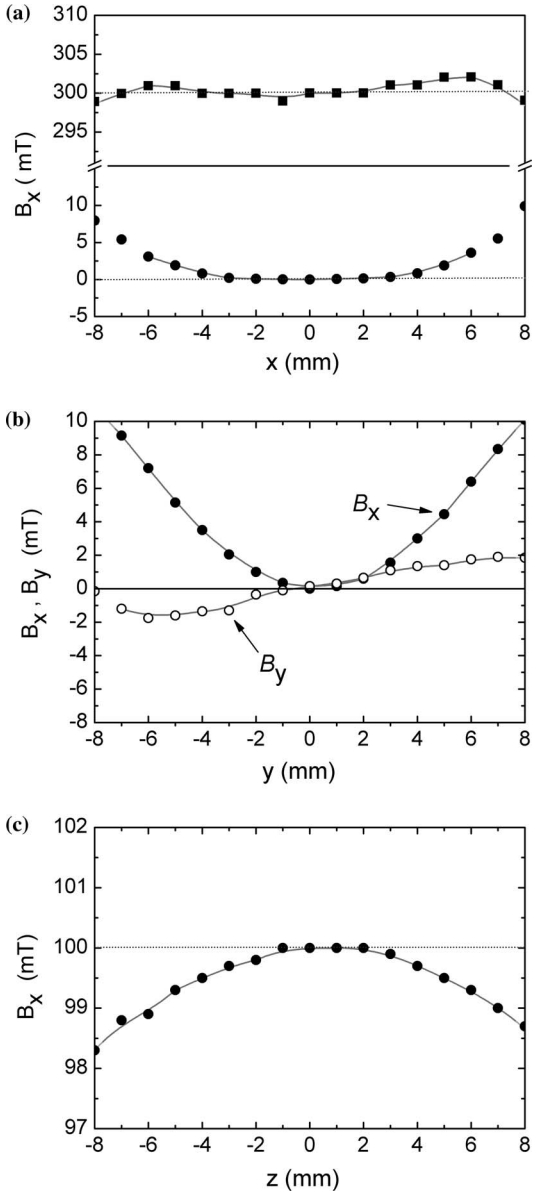

FIG. 9. (a) Magnetic field B_x (horizontal) as function of horizontal distance from the center for $B = 0$ mT and $B = 300$ mT. (b) B_x and B_y (vertical) as a function of the vertical distance y for $B = 0$ mT measured from the sample center. (c) Magnetic field B_x as function of the distance z from the center, i.e., perpendicular to the sample surface.

constant plateau of $B_x = 300$ mT ± 2 mT in between –8 mm $< x <$ +8 mm is observed (magnified scale see Fig. 9(a)). This interval exceeds the typical sample size of 10 mm × 10 mm – and more importantly – the scanning size of a light beam which is typically smaller than 3 mm × 3 mm. For huge as well as for very small magnetic fields the plateau of constant magnetic field strength is reduced to typically 4 mm × 4 mm which is, however, acceptable for practical applications.

At low magnetic fields the homogeneity is of interest, because the relative deviation can increase drastically. Figure 9(a) shows the magnified detail of the curve for $B_x = 0$ mT, taken from Fig. 8. The extension of the plateau is reduced, because the field increases to 1 mT at –3 mm and +3 mm. An enlargement of the plateau may be obtained

by an optimized alignment of the smaller magnetic rods with respect to the coupling requirement $\alpha_{1,3} = -\alpha_{5,7}$, $\alpha_{2,4} = -\alpha_{6,8}$, and $\alpha_{6,8} = \pi - \alpha_{5,7}$ (see Sec. II).

The degree of homogeneity of the magnetic field with respect to the vertical y-direction measured from the center is shown in Fig. 9(b) for $B_x = 0$ mT. For this situation both the horizontal field component B_x and the vertical field component B_y should be zero across a wide range. This is observed at the center within a region of few millimeters. An increase of this homogeneous region can be obtained by an improved alignment of the eight magnets. At this low field values the vertical component can create a critical distortion. Within the range –3 mm $< x <$ +3 mm the vertical field remains small with values below 1 mT.

The homogeneity in z-direction (Fig. 9(c)) for a nominal field $B_x = 100$ mT is nearly perfect across an 8 mm wide range due to the extension of the magnetic rods above and below the sample plane.

B. Magnetic field of type B

The magnetization device of type B (see Sec. II B) was designed for a continuous rotation of the magnetic field vector in the sample surface plane. This device shows a maximum magnetic field strength of 455 mT. The homogeneity of the magnetic field is of the same quality as obtained for device type A. These features will not be discussed in detail, but we will rather focus on the rotational behavior. A continuous rotation of the magnetic field vector is feasible across the range $0° \leq \gamma \leq 180°$ as shown in Fig. 10 for a field of 200 mT. During the full rotation the absolute value of the magnetic field is maintained within $\Delta B \leq 0.1$ mT. This accurate tuning of the field direction and value is achieved by the individual control of each motor driving the magnetic rods.

C. Investigation of magnetic layers

The potential and performance of the TetraMag magnetizing device is demonstrated by means of magneto-optical Kerr (MOKE) spectroscopy with synchrotron radiation. For this purpose, the TetraMag was implemented into a newly build ultrahigh vacuum compatible reflectometer.[14] During operation the vacuum was below 10^{-8} mbar. A magnetic multilayer sample with 30 alternating layers of (NiO 4 nm/CoFe 2 nm) on Si with a 5 nm Cu cap layer as oxidation protection was placed in the center of the magnetizing device (Figs. 6(a) and 6(b)).

The measurements were performed at the synchrotron facility DELTA in Dortmund at the bending magnet beamline 12. A toroidal grating monochromator provides mainly linearly polarized light with a degree of linear polarization $P_L = 0.9$ and a degree of circular polarization $P_C = 0.43$ in the energy range between 10 eV and 200 eV. The degree of polarization was determined on-site by a newly built Rabinovich detector. This detector is made up by a gold mirror set close to the Brewster angle and by a detector (GaAs:P-diode), both of which are rotated about the light beam (details see, e.g., Ref. 15).

The reflectivity spectra (Fig. 11) as a function of photon energy were taken in transverse (T-MOKE) geometry, i.e., a magnetic field oriented vertical to the scattering plane and within the sample plane. The light was linearly polarized in p-geometry, i.e., the electric field vector is oriented horizontally and thus pointing perpendicular to the magnetization direction of the sample and it is reflected in the horizontal plane.[2] The sample was set to 60° angle of incidence measured with respect to the surface plane. Due to the magneto-optical Kerr effect the reflectivity changes from R^+ to R^- upon switching the sign of the transversal magnetic field from $B = +100$ mT to $B = -100$ mT. The resultant spectra R^+ and R^- are used to deduce the T-MOKE asymmetry spectrum $A_T = (R^+ - R^-)/(R^+ + R^-)$, which exhibits clear structures of magnetic origin at the energy positions of the 3p absorption edges of Fe (54 eV), Co (60 eV), and Ni (66–68 eV) (Fig. 11 bottom).

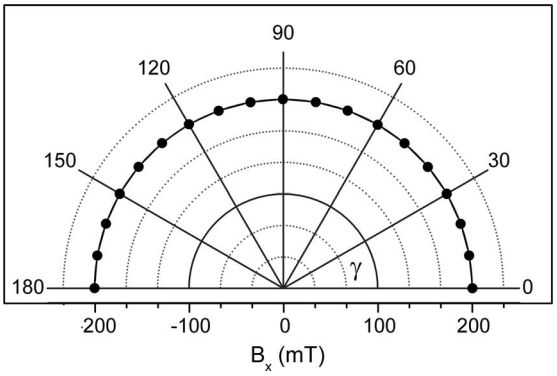

FIG. 10. Rotation of the magnetic field vector in the range $0° \leq \gamma \leq 180°$ while the absolute value is maintained shown for $B = 200$ mT.

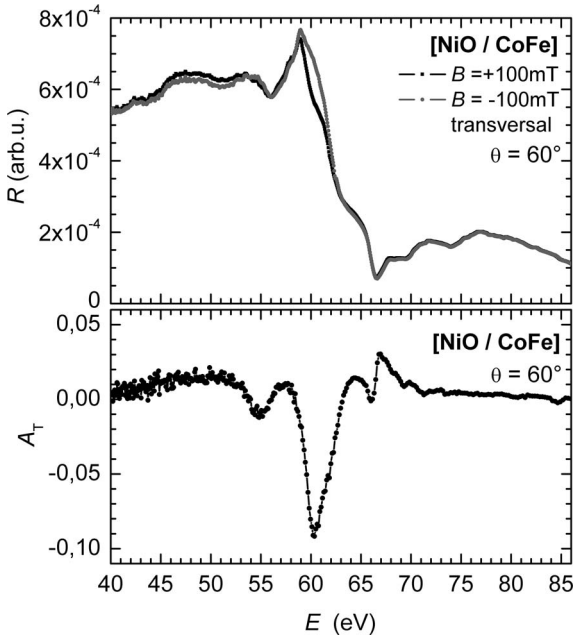

FIG. 11. T-MOKE spectra of a NiO/FeCo multilayer at 60° angle of incidence. Top: Reflectivity for transversal magnetization R^+ for $B = +100$ mT and R^- for $B = -100$ mT. Bottom: The T-MOKE asymmetry spectrum $A_T = (R^+ - R^-)/(R^+ + R^-)$ shows clear structures at the 3p resonances of Fe (54 eV), Co (60eV), and Ni (66–68 eV).

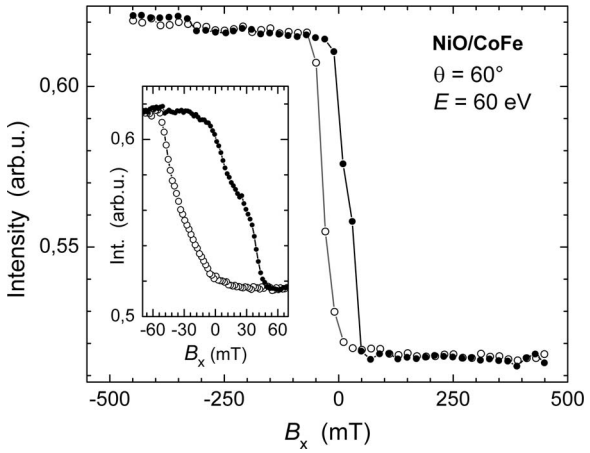

FIG. 12. Hysteresis curve of NiO/CoFe-multilayer system measured by monitoring the reflected intensity of synchrotron radiation at 60 eV photon energy and 60° angle of incidence.

A hysteresis curve (Fig. 12) was measured at the Co 3*p* edge at 60 eV, where a maximum magneto-optical response of the reflected light beam is observed. In this case, the reflected intensity was monitored as a function of the vertical magnetic field strength. The resultant hysteresis curve demonstrates the advantages of the quadrupole magnetizing device. First, clear noise-free signals can be obtained for a wide scanning range up to large magnetic field values. Second, data can be obtained also at small magnetic fields close to zero with a possible step width (resolution) of 0.02 mT (Fig. 12, inset). Additionally, measurements in L-MOKE geometry, i.e., with horizontally oriented magnetic field have been performed, yielding similar hysteresis curves (not shown). A detailed discussion of the magnetic sample and a comparison with different magnetic multilayers will be given in Ref. 14.

V. CONCLUSION

A novel quadrupolar magnetizing approach is presented and its usability is demonstrated by first magneto-optical measurements. The TetraMag device is based on eight NdFeB magnetic rods with magnetization direction perpendicular to their longitudinal axes. The rods are placed on the corners of two square profiles. Two different modifications have been presented. Type A couples all magnetic rods by a set of pinions and drives the magnets by one single motor. It allows for a tuning of magnetic fields between –570 mT and +570 mT with an accuracy and step width below 0.02 mT. The fields are homogeneous across the sample in all three directions. The second magnetization device type B exhibits an individual control of each magnet. This allows for a precise tuning of the magnetic field direction continuously from 0° to 180° while the magnetic field strength keeps unchanged.

The commissioning yielded experimental data of magnetic field strength and homogeneity which are in good agreement with our theoretical predictions. This versatile device avoids cooling mechanism and hysteresis effects known from classical electromagnets. It is ultra high vacuum compatible and it offers a completely free optical path over 180° for magneto-optical experiments. Thus, it is suited for scattering experiments with synchrotron radiation as well as with neutrons or for magnetic microscopy applications.

ACKNOWLEDGMENTS

We thank all staff members of the mechanical shops at the University of Applied Sciences, Münster and Forschungszentrum, Jülich for support in construction and for manufacturing of the magnetization devices. We acknowledge the technical support by Ulf Berges at DELTA. This work was supported financially by the "Ministerium für Innovation, Wissenschaft und Forschung des Landes NRW."

[1]M. Mansuripur, *The Physical Principles of Magneto Optical Recording* (Cambridge University Press, Cambridge, England, 1998).
[2]H.-Ch. Mertins, S. Valencia, A. Gaupp, W. Gudat, P. M. Oppeneer, and C. M. Schneider, Appl. Phys. A **80**, 1011 (2005).
[3]A. Hubert and B. Schäfer, *Magnetic Domains* (Springer-Verlag, Berlin, Germany, 1998).
[4]Th. Du Moncel, *Elements of Construction for Electro Magnets*, Reprint (BiblioBazar, Charleston, South Carolina, 2008).
[5]E. Arenholz and S. O. Prestemon, Rev. Sci. Instrum. **76**, 083908 (2005).
[6]C. S. Hwang, C. T. Chen, C. H. Chang, C.-Y. Liu, F. Y. Lin, B. Wang, and R. Wahrer, J. Magn. Magn. Mater. **239**, 586 (2002).
[7]H. A. Dürr, T. Eimüller, H.-J. Elmers, S. Eisebitt, M. Farle, W. Kuch, F. Matthes, M. Martins, H.-Ch. Mertins, P. M. Oppeneer, L. Plucinski, C. M. Schneider, H. Wende, W. Wurth, and H. Zabel, IEEE Trans. Magn. **45**, 15 (2009).
[8]O. Cugat, R. Byrne, J. McCaulay, and J. M. D Coey, Rev. Sci. Instrum. **65**, 11 (1994).
[9]K. Halbach and L. Berkeley, Nucl. Instrum. Methods **169**, 1 (1980).
[10]COMSOL© is a commercial available multiphysics modeling and simulation software.
[11]J. D. Jackson, *Classical Electrodynamics* (Wiley, New York, 1998).
[12]Klüberalpha HPX 93-1202, Datasheet, Klüber Lubrication KG, Munich, Germany, 2008.
[13]Melexis MLX90215, Datasheet, NV Melexis SA, Ieper, Belgium, 2009.
[14]M. Tesch, M. Gilbert, H.-Ch. Mertins, and C. M. Schneider, XMAPS: a multi-purpose device for eXtended Magneto-optical Polarization Spectroscopy in the visible, EUV- and soft X-ray region (to be published).
[15]F. Schäfers, H.-Ch. Mertins, A. Gaupp, W. Gudat, M. Mertin, I. Packe, F. Schmolla, S. Di Fonzo, G. Soullié, W. Jark, R. Walker, X. Le Cann, M. Eriksson, and R. Nyholm, Appl. Opt. **38**, 4074 (1999).